Spray Coating Experiments: Setups and Methodologies

The latest eBook from Advanced Optical Metrology. Download for free.

Spray Coating Experiments: Setups and Methodologies, is the third in our Thin Films eBook series. This publication provides an introduction to spray coating, three article digests from Wiley Online Library and the latest news about Evident's Image of the Year Award 2022.

Wiley in collaboration with Evident, are committed to bridging the gap between fundamental research and industrial applications in the field of optical metrology. We strive to do this by collecting and organizing existing information, making it more accessible and useful for researchers and practitioners alike.

EVIDENT
OLYMPUS

WILEY

ADVANCED FUNCTIONAL MATERIALS
www.afm-journal.de

Contactless Pulsed and Continuous Microdroplet Release Using Photothermal Liquid Crystals

*Pinar Beyazkilic, Samet Akcimen, Caglar Elbuken, Bülend Ortaç, Shengqiang Cai, and Emre Bukusoglu**

Targeted, on-demand delivery has been of interest using materials responsive to environmental stimuli. A delivery technique based on precise release of aqueous microdroplets from a liquid crystal (LC) medium with contactless stimulation is presented. A nematic LC is doped with a photothermal dye that produces heat under near IR light exposure. The heat is used to overcome the elastic strains in the LC phase, promoting the release of initially entrapped water droplets to the neighboring aqueous solution. Designing the geometry of LC-based emulsions and tuning the light intensity and position allows for manipulation of the release in two distinct modes defined as pulsated and continuous. In the pulsated mode, water droplets are released transiently from the casted water-in-LC emulsion layer based on sweeping by the moving isotropic-nematic phase boundary controlled by light. In the continuous mode, water droplets are ejected continuously from a droplet-shaped water-in-LC emulsion, due to a heating-induced internal flow controlled by light. The droplet release by contactless stimulation is used for the on-demand dosing of dopamine and its oxidizing reagent from isolated reservoirs to obtain an in situ reaction signal for a hydrogen peroxide assay. A new dual-mode release system developed with photothermal LCs holds potential in drug release, controlled mixing, and photothermal therapy.

1. Introduction

Controlled release of substances is highly desirable due to the side effects arising from high dosing and uptake rates.[1–3] Stimuli-responsive systems have been developed, which enable the agents to be released on-demand by environmental stimulations such as light, heat, or pH.[4–8] Most of such systems have been designed with gatekeeper mechanisms made from soft materials (e.g., polymers, lipid bilayers among the others) that expel the agents at the specific target sites through melting or degradation processes triggered by external stimuli.[9–14] However, once opened, the "gates" cannot be recovered to stop the release, therefore, there is need for the systems with precise control of phase change that enables a reversible start–stop release mechanism.

Liquid crystals (LCs) are an emerging class of materials that found applications in diverse fields beyond display devices including optical biosensors, actuators, and liquid manipulation owing to the unique structural and optical properties such as elastic anisotropy arising from molecular orientation, reversible phase change, and birefringence.[15–23] LCs can flow and exhibit mesoscale ordering. They can be designed to switch from anisotropic (ordered) to isotropic state under various stimuli including electric field, heat, and solvent.[24,25] A recent concept has been reported describing the release of droplets from thermotropic nematic LCs.[26] Specifically, during phase transition, the boundary between isotropic phase and nematic LC phase (I-N phase boundary) breaks the balance between the buoyancy and elastic repulsion forces arose in LC medium, and moves the dispersed, micrometer-scale water droplets toward the aqueous phase boundary as cargo expulsed to the external aqueous solution. The transition from LC to isotropic phase was achieved by contact heating. In other approaches, droplets were released by applying chemical stimuli or by bacterial motion-induced shearing on the LC-aqueous phase interfaces.[26] However, contactless stimulation of such release systems offers unique features in targeted delivery applications such as ease-of-handling, remote controllability, and rapid and repetitive on/off control.

LCs were previously hybridized with fluorescent dyes,[27–29] azobenzene molecules,[30–32] gold nanoparticles,[33,34] and

P. Beyazkilic, E. Bukusoglu
Department of Chemical Engineering
Middle East Technical University
Dumlupınar Bulvarı No:1 Çankaya, Ankara 06800, Turkey
E-mail: emrebuk@metu.edu.tr
S. Akcimen, C. Elbuken, B. Ortaç
Institute of Materials Science Nanotechnology
National Nanotechnology Research Center (UNAM)
Bilkent University
Ankara 06800, Turkey
C. Elbuken
Faculty of Biochemistry and Molecular Medicine
Faculty of Medicine
University of Oulu
Oulu 90014, Finland
S. Cai
Department of Mechanical and Aerospace Engineering
Materials Science and Engineering Program
University of California, San Diego
La Jolla, CA 92093, USA
The ORCID identification number(s) for the author(s) of this article can be found under https://doi.org/10.1002/adfm.202205385.

DOI: 10.1002/adfm.202205385

magnetic nanoparticles[35,36] to design platforms responsive against noncontact electromagnetic sources including ultraviolet light, near infrared (NIR) light, or magnetic field. NIR light presents particular advantages that include localized exposure, high penetration depth, and low power intensity, which hold significant importance in biomedical fields.[37] Furthermore, NIR light is converted to heat when absorbed by photothermal agents, therefore it has been extensively used in various heat-mediated applications ranging from photothermal therapy and imaging to actuators and soft robotics.[38–43] Release of microdroplets which was previously accomplished by applying contact heating or chemical stimuli on the LCs, provides limited spatial control since heat (contact) and chemicals diffuse over the entire LC-aqueous phase interfaces.[26] In addition, triggering effect induced by chemicals can take time to cease. Light-induced release on the other hand, offers spatiotemporal precision with localized excitation as well as the prompt removal of the excitation.

Herein we introduce a microdroplet release method based on NIR excitation using photothermal dye-doped nematic LC. Local excitation combined with rapidly adjustable heating rate and precise on/off control provided by using light, realized a more localized stimulation and spatiotemporally controlled release. 4-Cyano-4′-pentylbiphenyl (5CB), a generic, thermotropic LC, was physically hybridized with *N*,*N*,*N*′,*N*′-tetrakis(*p*-disobutylaminophenyl)-*p*-phenylenediimmonium bis(oxalato) borate (PDIB) dye by a solvent-aided mixing. LC-based release system was prepared by emulsification of aqueous (dye-loaded) cargo droplets into photothermal dye-hybridized LC, followed by casting the emulsion on an aqueous phase. Microdroplet release was accomplished remotely by illuminating an NIR laser on the LC surface that generates heat through the photothermal process of the PDIB dye. LC transited to isotropic phase due to the photothermal heating and water droplets in the nematic phase were released to the aqueous solution in a pulsated fashion due to the advancing I-N phase boundary. A next release pulse occurred after consecutive laser-off and -on actions. The total released mass was controlled at the microgram level by the number of repeated heating-cooling cycles. Adjustable laser beam spot size and LC dimension provided a precise setting of the released mass in a single pulse. Surprisingly, we also obtained a localized, continuous-mode release by using the same stimulation source but a distinct LC geometry. Local heating of a droplet-shaped water-in-LC compartment by NIR light beam generated a temperature gradient that resulted in an internal flow leading to the shearing-based droplet release through the aqueous phase boundary. Flow-induced release is superior to those created by chemical or contact heating with instantaneous in situ adjustment of the release by tuning the laser intensity. Beyond dual-mode operation, contactless heating combined with beam spot size adjustability (1–9 mm) offered flexibility in using LC with various sizes and shapes (e.g., circular, rectangular, droplet), and enabled remotely controlled mixing of the reagents used for chemical assays, which we demonstrated in an exemplary assay.

2. Results and Discussion

Scheme 1 illustrates the pulsated release principle by using the contactless heating. Water microdroplets containing red tracer dye and 9×10^{-3} M sodium dodecyl sulfate (SDS) used for homeotropic LC anchoring were initially emulsified in nematic LC phase (see Experimental Section). Escape of the droplets to a neighboring aqueous phase is blocked by a mechanism that is associated with the elastic forces on the droplets applied by LC as described previously (Scheme 1a).[] When NIR light was illuminated on photothermal dye-LC hybrid on its air-LC interface, temperature reached above nematic-to-isotropic phase transition temperature (T_{NI}) through photothermal heating. Due to the

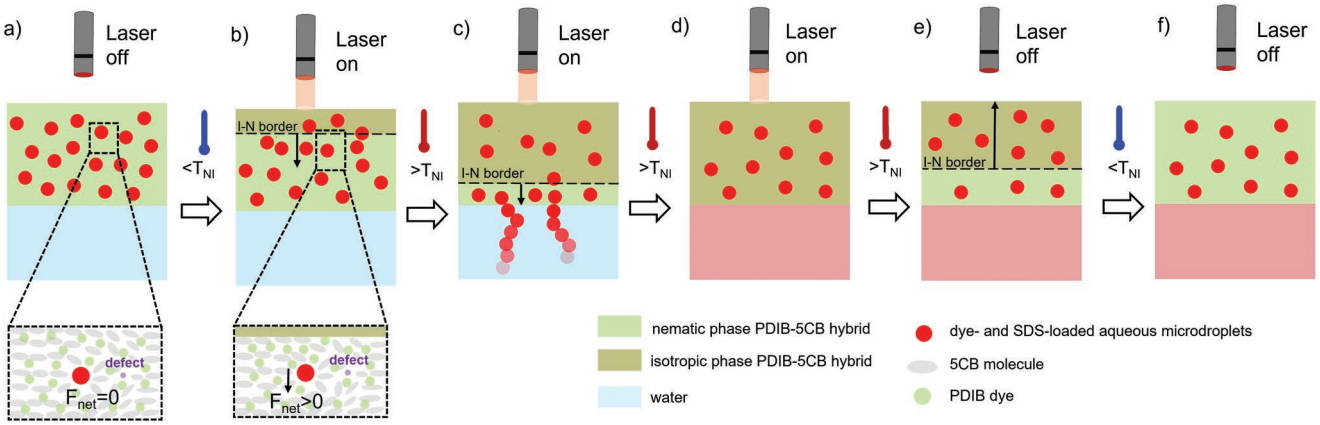

Scheme 1. Illustration of NIR-responsive pulsated-release of aqueous microdroplets from PDIB-hybridized nematic LC based on photothermal heating and LC phase change. T_{NI} denotes the nematic-to-isotropic phase transition temperature. a) Aqueous microdroplets levitated in nematic LC at laser-off state. Close-up view represents the defect formed due to the competition between the elastic strain of LC and orientation energy at the droplet interface and zero net force (F_{net}) due to the balance between elastic strain exerted on the microdroplet and buoyancy force. b) Transition to isotropic phase due to the photothermal heating at laser-on state and expansion of isotropic-nematic (I-N) boundary toward the aqueous interface and sweeping of microdroplets by the I-N boundary. Close-up view represents the increasing of (F_{net}) on the microdroplet due to elastic force exerted by the moving I-N boundary. c) Release of the droplets at the aqueous interface due to the defeating of elastic barrier at the aqueous interface by the approaching I-N boundary. d) Complete transition from nematic phase to isotropic phase. e) Movement of I-N boundary in the reverse direction at laser-off state due to cooling started at the aqueous interface. f) Complete transition from isotropic phase back to nematic phase.

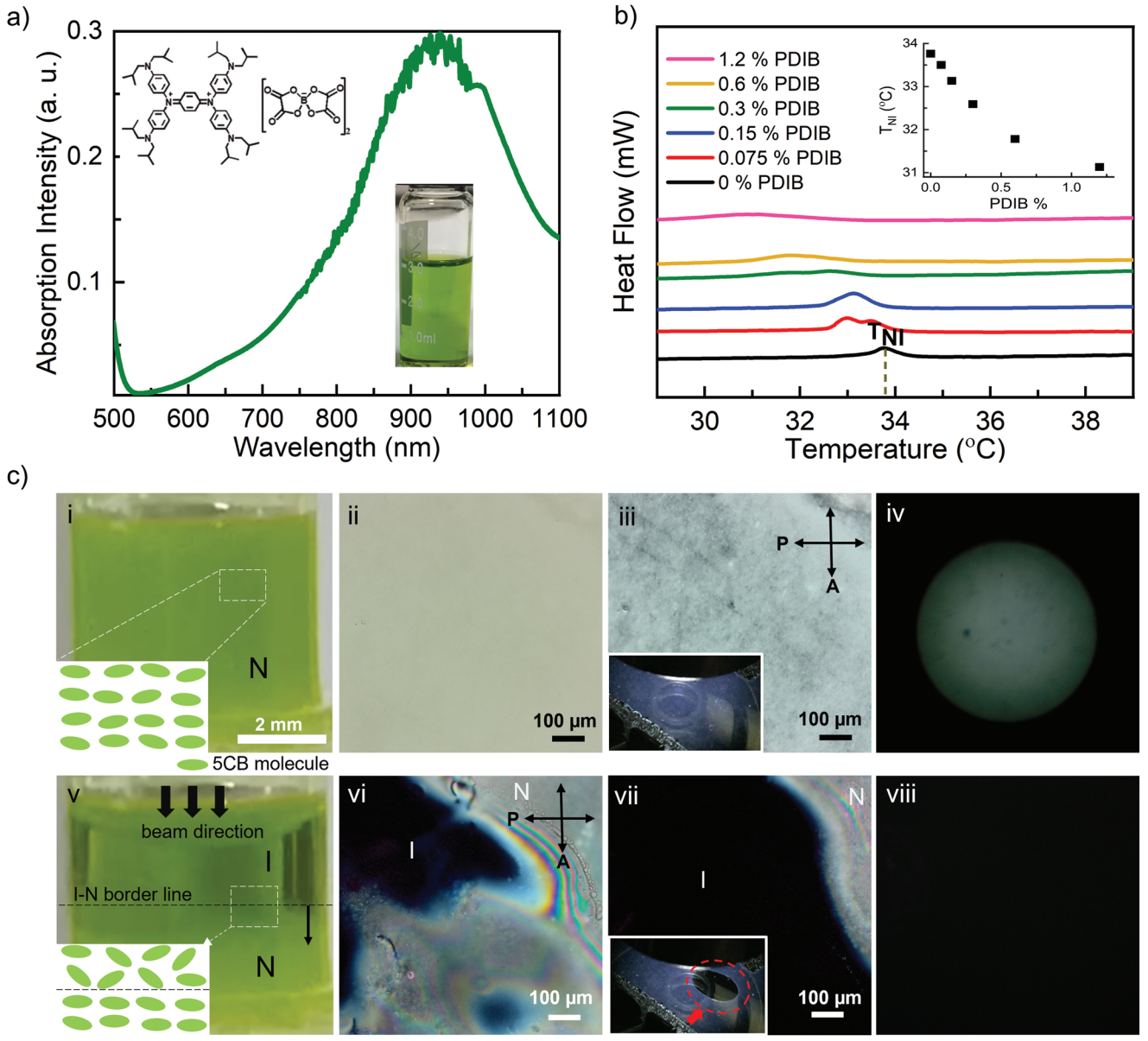

Figure 1. a) Absorption spectrum of PDIB solution. Inset shows a picture of PDIB solution in toluene, and chemical structure of PDIB (with molecular formula $C_{62}H_{90}N_6$ $(BC_2O_4)_2$). b) Differential scanning calorimetry thermographs of pure 5CB, and PDIB-5CB mixtures with 0.075, 0.15, 0.3, 0.6, and 1.2 wt.% PDIB loading. Inset shows the change of T_{NI} with increasing PDIB loading. c) i) PDIB-5CB hybrid mixture in a plastic reservoir of 5 mm diameter and 5 mm height. Inset represents the nematic (N) ordering of the 5CB molecules at room temperature. ii) Bright field microscopy and iii) POM images of PDIB-5CB hybrid sandwiched between glass slides, iv) conoscopic image taken with Bertrand lens before exposure to NIR laser. Arrows named as P and A show the direction of polarizer and analyzer, respectively. v) PDIB-5CB hybrid mixture illuminated with a 3 mmspot sized laser beam from the top. Dashed black line represents I-N phase boundary moving down. Inset represents the ordering of the 5CB molecules in isotropic (I) phase and neighboring nematic phase in the dashed rectangle. vi,vii) POM and viii) conoscopic images of sandwiched PDIB-5CB film during exposure to NIR laser. Insets in (iii) and (vii) show the photographs of the film located under the objective before and during exposure to NIR laser, respectively. Red dashed circle in (vii) shows the transparent region which is isotropic due to the photothermal heating.

thermal diffusion process, isotropic phase progressively expanded toward the aqueous interface (Scheme 1b). This moving I-N phase boundary applies elastic forces and sweeps a certain portion of the droplets in the nematic phase (Scheme 1b).[26] When I-N boundary approached the aqueous interface, the droplets at the aqueous interface were released and merged with the aqueous solution while the rest were suspended in the isotropic phase (Scheme 1c,d). The reason was previously explained by the higher drag force exerted to the larger sized droplets in the opposite direction to their movement.[26] If the drag force overcomes the net moving force on the droplets, droplets contact the moving I-N boundary leading to their expulsion to the isotropic phase.[26] After the laser was turned off, nematic phase was recovered back due to the lower surrounding temperature (Scheme 1e,f).

We synthesized the photothermal PDIB dye (**Figure 1**a) following the procedure described in a previous report[46] and

characterized using FTIR and XPS as shown in Figures S1 and S2 (Supporting Information). PDIB formed a green solution when dissolved in organic liquids and exhibited a strong absorption peak around 930 nm (Figure 1a, inset shows a photograph of PDIB dissolved in toluene). NIR light within 650–900 nm range can penetrate in biological tissues within 1 cm-depth, and therefore is widely used in biomedical applications.[47] The absorption spectrum of PDIB matches well with the wavelength of NIR light for such applications. In this study, a diode laser with 915 nm-wavelength was used to maintain both high absorbance and safer operating condition with lower photon energy compared to that of shorter wavelengths. Decomposition temperature of PDIB was measured to be 298 °C using thermogravimetric analysis (Figure S3, Supporting Information), enabling a wide thermal operating range. PDIB was physically hybridized with 5CB by mixing both in toluene and subsequently evaporating toluene under vacuum. T_{NI} of PDIB-5CB hybrid mixtures was measured using a differential scanning calorimeter. T_{NI} of pure 5CB was 33.8 °C, which gradually shifted from 33 to 31 °C by increasing PDIB concentration from 0.075 wt.% to 1.2 wt.% (Figure 1b). The decrease of T_{NI} was attributed to the slight disruption of the LC phase with increasing dye that was similarly observed with the addition of halogen-bonded dye to 5CB.[48]

Importantly, homogeneous green color of the PDIB-5CB hybrid filling a reservoir of 5 mm diameter and 5 mm height confirmed the fine dispersion of PDIB (Figure 1c(i)). Furthermore, optical microscopy images revealed no PDIB aggregate formation (Figure 1c(ii)). Absorption intensities of PDIB in several locations of the hybrid mixture were also close to each other proving the homogeneous PDIB dispersion (Figure S4, Supporting Information). The opaqueness observed in Figure 1c(i), polarized light transmission through the PDIB-5CB hybrid film (Figure 1c(iii)) and conoscopic image taken with Bertrand lens (Figure 1c(iv)) revealed the nematic ordering of 5CB at room temperature. The hybrid mixture was illuminated with a 3 mm-spot sized laser beam from the top. Appearance of the transparent green coloring at the top regions indicated the transmission of PDIB-5CB mixture to isotropic phase via photothermal process (Figure 1c(v)). Top isotropic phase was distinguishable from the bottom nematic phase by the spatial abrupt change in transparency observable with naked eyes. The line where transparent LC was separated from the opaque part was the so-called I-N phase boundary (Figure 1c(v)). I-N phase boundary moved vertically down until 5CB was completely turned to isotropic with prolonged heating. Transition to isotropic phase was also observed by the gradual expansion of dark appearance in polarized optical microscope (POM) and conoscopic images (Figure 1c(vi–viii)). Isotropic area on the hybrid film was seen as a transparent region in ellipse shape as denoted with red dashed circle in Figure 1c(vii). The shift velocity of the I-N phase boundary was determined using an image analysis software (ImageJ) after recording the video of mixture shown in Figure 1c(v) under laser exposure. When laser power was increased from 94 to 184 mW for the 3 mm-spot sized NIR beam, the velocity increased from 0.02 to 0.03 mm s^{-1} (Table S1, Supporting Information). When the beam spot size was decreased from 3 to 2 mm for the power of 94 mW, the velocity decreased from 0.02 to 0.003 mm s^{-1} that can be explained by the decreased spatial heating rate (Table S1, Supporting Information).

Another unique feature of the presented release system is the precise tunability of the heating rate. To investigate the heating rate with varying laser power intensity and PDIB loading, temperatures of PDIB-5CB mixtures were recorded using a thermal camera. Temperature of the hottest spot (NIR exposed top region of the sample) denoted by the "$+_1$" sign on the thermal map was recorded as shown in representative images in **Figure 2**a. Temperature was measured on PDIB-5CB for 120 s under exposure to a 3 mm-spot sized laser beam at different laser intensities. Temperature reached to the T_{NI} ≈32 °C (for 0.15 wt.% PDIB loading) in 30 s at a laser intensity of 0.9 W cm^{-2} and same temperature in less than 5 s at 3.5 W cm^{-2} (Figure 2b). Heating rate and maximum temperature increased with an increase in the laser intensity and PDIB loading (Figure 2c; Figures S5 and S6, Supporting Information). When PDIB content was increased from 0.075 wt.% to 0.15 wt.% under exposure to the 3 mm-spot sized beam with a power of 184 mW, the shift velocity of the I-N phase boundary increased from 0.003 to 0.01 mm s^{-1} that was attributed to the higher light absorption (Table S1, Supporting Information). As shown in Figure S7 (Supporting Information), the absorption intensity of the PDIB-5CB hybrid mixture increased with increasing PDIB concentration. PDIB-5CB showed reversible photothermal heating against repeated laser-on actions as demonstrated with five successive heating-cooling cycles where cooling took place passively at room conditions in the laser-off state (Figure 2d). No significant changes in the heating rate or maximum temperature were observed after the repeated measurements indicating the significant stability of the dye in 5CB and a non-hysteretic operation of the presented release system.

Based on the propagation of the isotropic phase throughout the LC, an NIR-responsive microdroplet release system was designed. The system is a water-in-LC emulsion prepared by loading red-dyed water droplets in PDIB-5CB mixture. Size distribution of the aqueous microdroplets was found to be in the range of 2–120 µm (averaging around 20 µm) using optical microscopy images of the water(dyed)-in-PDIB/5CB emulsions and ImageJ software (Figure S8, Supporting Information). **Figure 3**a shows the photothermal LC emulsion placed at the bottom of a glass tube filled with water and turned upside down. The emulsion was excited with the laser beam from the glass side. The generated I-N phase boundary was propagated toward the aqueous phase and clearly showed the suspended, red microdroplets in PDIB-hybridized green 5CB. Because of the I-N phase boundary shift, the dyed droplets were released into the water underneath. 5CB remained structurally intact during the release, unlike many other gatekeeper materials that undergo structural disruption to release the agents under stimuli.[9–14] A consecutive release pulse was also achieved by turning off the NIR light to allow the LC to transit back to the nematic phase and then turning on the laser again (Video S1, Supporting Information).

To investigate the characteristics of the NIR-induced, pulsated release in more detail, we casted water(dyed)-in-PDIB/5CB emulsions on aqueous solutions in cuvettes of 4 mL volume through mini-wells and left their top open to air. For this, the emulsions were filled in square or circular shaped gaps of

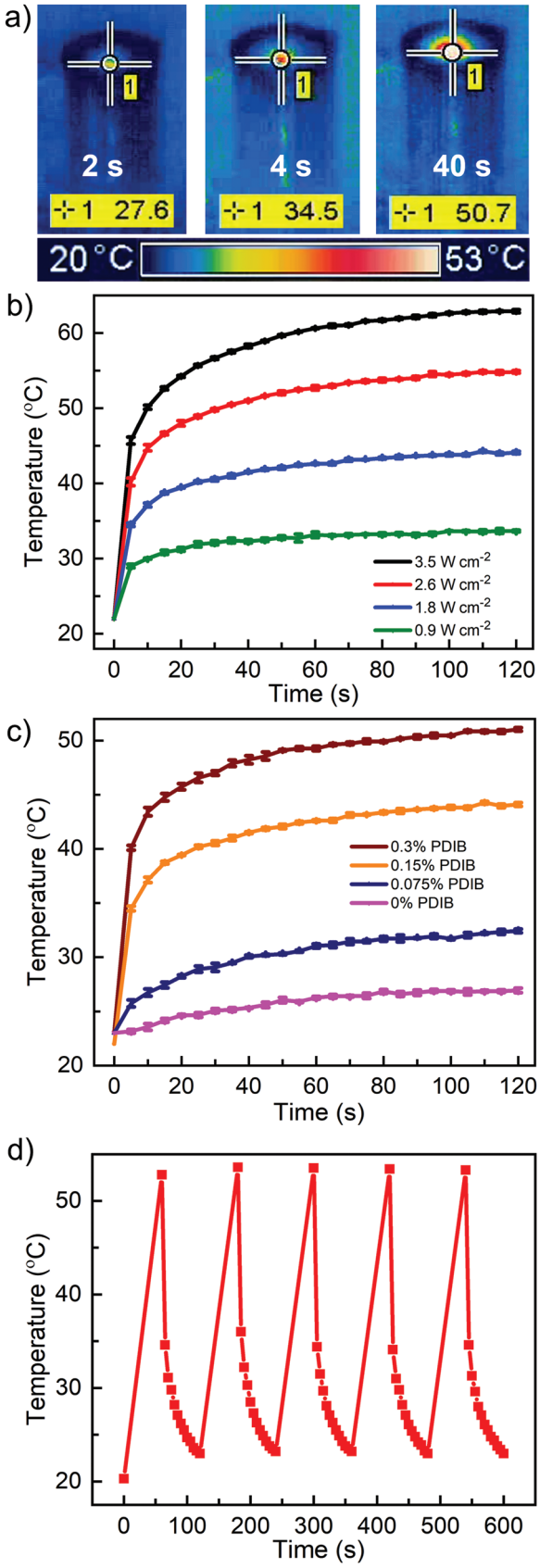

various surface areas formed in PDMS molds (Figure 3b). The emulsions were excited from their top with a 9 mm-spot sized laser beam at an intensity of 0.7 W cm^{-2}. Release performance of the hybrid emulsions was investigated by analyzing the mass of released red ponceau dye with spectrophotometry after seven laser on/off cycles. Beam spot size was kept larger than the mini-well area occupied by LC emulsion for homogenous exposure. Consistently, cumulative released mass increased with sequential pulses, which was also increased linearly depending on the increasing LC area (Figure 3c,d). The lower release rate with smaller area was also obvious upon visual monitoring (Figure 3b). Interestingly, we observed release to occur near the edges of the LC. Cross-sectional imaging of LC revealed a meniscus where LC was thicker near the PDMS walls (Figure 3e). Thus, the total droplet population along the height of the emulsion was higher toward the PDMS walls. The reason of the evident release at the edges was ascribed to the further population of the droplets near the edges of the emulsion with the moving dome-shaped isotropic phase (Figure 3e, schematic view of the PDMS-LC-aqueous phase interface). The formation of the dome-shaped isotropic phase was attributed to the slower penetration of NIR light at the thicker edges. Consequently, the sweeping of the droplets in the same direction with the motion of the I-N phase boundary can concentrate droplets near the edges resulting in a more pronounced local release there. We also found the cumulative released mass to increase linearly with the LC thickness at constant area (Figure 3f) since higher droplet congestion occurred due to the collection of droplets from a larger volume by the moving I-N border. Maximum released mass ratio for the total seven release pulses was found to be 15.4% on average. Release starting time after the laser was turned on depended on the laser intensity and the LC thickness while the LC area had a negligible effect. For instance, release was observed after 71 and 76 s in 1 mm-thick 0.07 and 0.19 cm^2 LC, respectively at 0.7 W cm^{-2} intensity. Release was observed after 118 s when the thickness was increased from 1 to 3 mm for the 0.19 cm^2 LC and after 30 s when the excitation intensity was increased from 0.7 to 1.4 W cm^{-2} for the 1 mm-thick 0.19 cm^2 LC. Thus, an increase in the light intensity consistently led to an increase in the heating rate and the velocity of the I-N phase boundary while the increase in thickness extended the path through which I-N boundary moved. It is noteworthy that release dosage was controlled from 0.5 to 2.5 µg per pulse and the total dosing was dependent on the number of the pulses.

Figure 2. a) Time-dependent thermal camera images of PDIB-5CB mixture (with 0.15 wt.% PDIB) dropped on a PDMS mini-well on the top of a glass cuvette. Temperature values on the spot (top region of the sample exposed to the laser beam) denoted by "+1" sign on the thermal maps are indicated in the corresponding yellow boxes. b) Temperature of PDIB-5CB (with 0.15 wt.% PDIB) measured every 5 s for 120 s under exposure to the 3 mm-spot sized laser beam at different laser power intensities ($n = 3$). c) Temperature of PDIB-5CB and plain 5CB measured every 5 s for 120 s under exposure to the 3 mm-spot sized laser beam at an intensity of 1.8 W cm^{-2} for different PDIB loading ($n = 3$). d) Temperature of PDIB-5CB (with 0.15 wt.% PDIB) measured during five consecutive heating–cooling cycles by exposing to the laser beam at an intensity of 2.6 W cm^{-2}. Temperature values were recorded at room condition with a temperature of 21 °C.

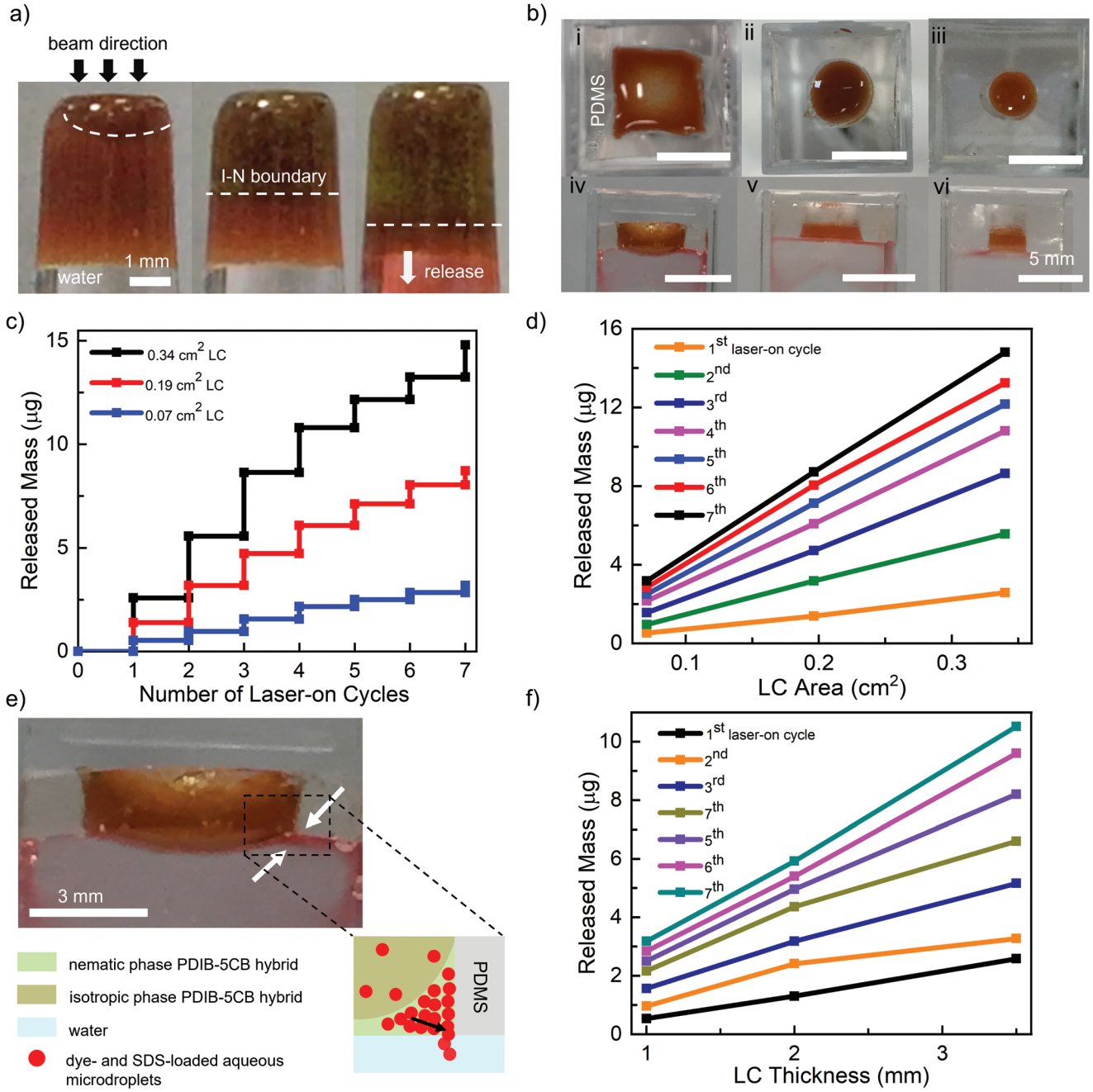

Figure 3. a) Water-in-LC emulsion prepared by loading red-dyed water droplets in PDIB-5CB hybrid. The emulsion was sequestered between the bottom of a glass tube and water and excited with a 3 mm-spot sized laser beam from the glass side. White dashed line shows the isotropic-nematic (I-N) border moving toward the aqueous phase underneath and allowing the red droplets to merge with the aqueous phase. b) i–iii) Top-view and iv–vi) side-view of water-in-LC emulsions casted on mini-wells with area of 0.34, 0.19, and 0.07 cm^2, respectively. c) Release profiles depending on the number of laser on-off cycles for different LC area. The horizontal period indicates the absence of release in between two consecutive laser-on cycles after the pulsated mass only once. d) Dependence of the cumulative released mass on the LC area for seven laser-on cycles. e) Side-view of water-in-LC emulsion during release. The dense red color on the edge between the white arrows shows the released dye. Scheme represents the droplet profile at the PDMS-LC-aqueous phase interface. f) Dependence of the cumulative released mass on the LC thickness with constant LC surface area (0.07 cm^2) for seven laser-on cycles. Emulsions were under illumination with a 9 mm-spot sized beam at an intensity of 0.7 W cm^{-2}. Released mass values represent red dye amount in micrograms (μg) in 4 mL of water.

Adjustment of the beam spot size on a relatively larger LC area resulted in the spatial control of the propagation of the isotropic phase and released droplet mass in pulsated release. As shown in **Figure 4**a(ii–iv, left images), evident green color of the area exposed to a 7 mm-spot-sized NIR beam indicated a reduced droplet density in the expanded dome-shaped isotropic phase due to the sweeping towards the outer regions by the moving I-N phase border. A schematic of the time-dependent

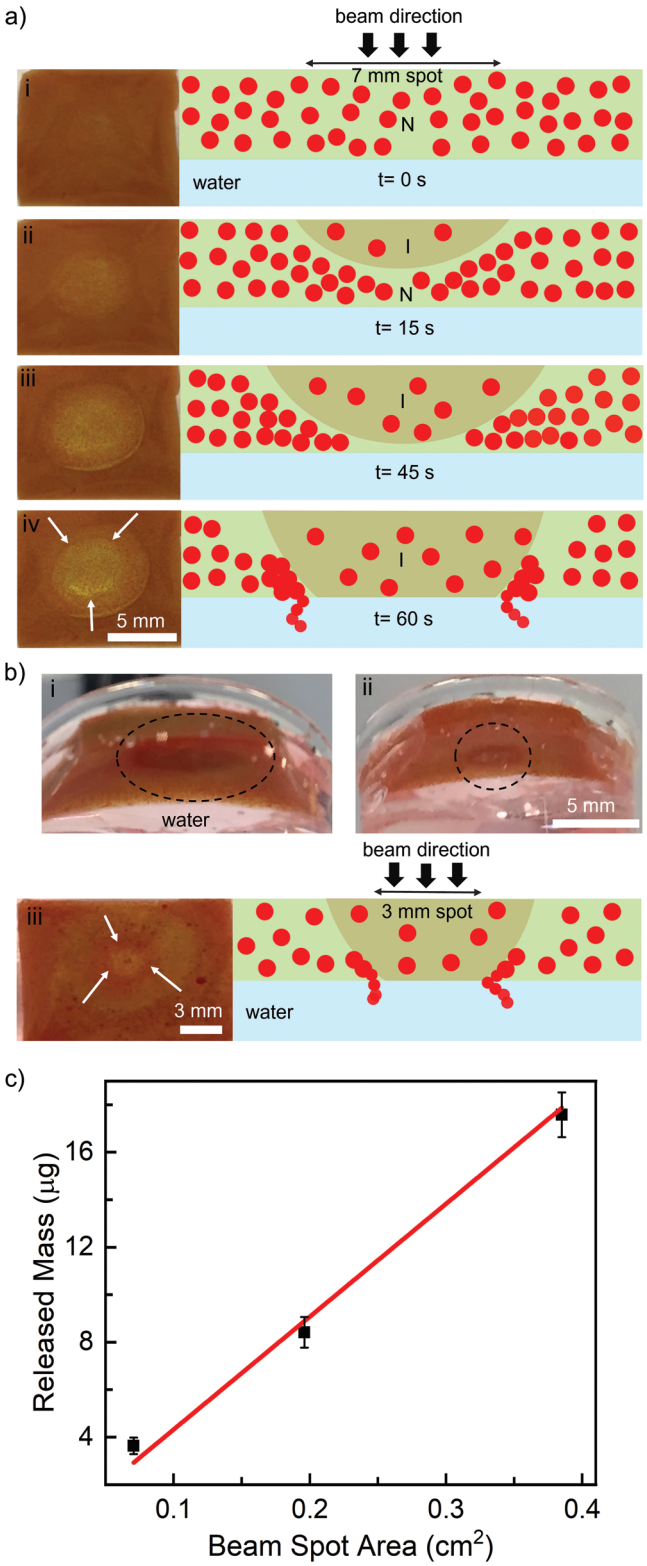

Figure 4. a) i–iv, left) Top-view of large-area water-in-LC emulsion under time-dependent heating by the excitation with a 7 mm-spot sized laser beam. White arrows denote the red ring-shaped droplet crowd released from the I-N-aqueous phase interface. i–iv, right) Corresponding schematic representation of the droplet (denoted as red spheres) profiles at the cross-section of emulsion. I and N represent the isotropic and nematic phases, respectively. b) View of the water-in-LC emulsions from their bottom surface showing the ring-shaped released droplet crowd in black dashed circles during the excitation with a i) 7 mm-spot sized or ii) 3 mm-spot sized beam. iii) Top-view and corresponding cross-sectional representation of the water-in-LC emulsion during the excitation with a 3 mm-spot sized laser beam. White arrows denote the red ring-shaped droplet crowd released from the I-N-aqueous phase interface. c) Linear fitting of released mass as a function of beam spot area. Release mass was measured after seven consecutive release pulses for each beam spot area ($n = 3$). Mass values represent red dye amount in micrograms (μg) in 4 mL of water.

movement of the I-N phase border and droplet distribution are shown in Figure 4a(ii–iv, right sketches). A droplet congestion was observed to occur in a ring pattern surrounding the green circle (Figure 4a(iii)). Droplet congestion was increased at I-N-aqueous phase interface by further propagation of the I-N boundary as evident from the darker red appearance around the green circle. The expansion of the isotropic phase defeated the elastic repulsion force on the droplet crowd adjacent to the aqueous border, therefore, led to their escape to the aqueous phase through a ring pattern (Figure 4a(iv)). Release of the dye was evident as a dense red ring with a diameter of ≈7 mm when observed from the top as denoted with the white arrows in Figure 4a(iv). Difference between the size of the ring-shaped droplet crowds upon illumination with an either 7 mm- or 3 mm-spot sized beam was also distinguishable when the emulsions were imaged from their bottom side (Figure 4b(i,ii)). A ring pattern of ≈3 mm diameter formed under exposure to a 3 mm-spot sized beam was also viewed from the top as denoted with white arrows in Figure 4b(iii). Consequently, site and size of the droplet gathering, and release were spatially controlled by the beam spot size when the spot area was smaller than the emulsion area. Through these experiments, we found the total released mass after seven consecutive pulses to increase linearly with the beam spot area ranging from 0.07 cm^2 for 3 mm spot size to 0.38 cm^2 for 7 mm spot size (Figure 4c).

We demonstrated the versatility of the microdroplet release system for on-demand mixing of the reagents to obtain their *in-situ* generated reaction signal. In situ polymerization of dopamine (DA) was shown for the quantitative hydrogen peroxide (H_2O_2) assay. H_2O_2 is an extensively used chemical and produced in various enzymatic processes (e.g., glucose oxidation).[49–51] DA is rapidly oxidized to quinone at basic pH and produces polydopamine (PDA) by undergoing several chemical and physical bonding interactions.[52,53] In the presence of H_2O_2, in situ generated PDA fluorescence increases due to scavenging reactions between peroxy-radicals and PDA.[54] We prepared an array of mini-wells of 5 mm diameter and 4 mm height and placed it above the H_2O_2 solution. Mini-wells were loaded with two separate water-in-LC emulsions loaded with DA and Tris-HCl (pH 8.6) buffer droplets (**Figure 5**a, inset). Buffer and DA droplets were released and mixed with the H_2O_2 solution in sequence (Figure 5a,b). Aqueous phase maintained a pink hue after the release due to the presence of the tracer red dye within the droplets and then turned to brown after PDA generation (Figure 5c). The fluorescence of PDA was centered around 490 nm and its intensity was found to increase with increasing H_2O_2 concentration from 1 to 5×10^{-3} M (Figure 5d). We note here that a prolonged PDA incubation upon premixing

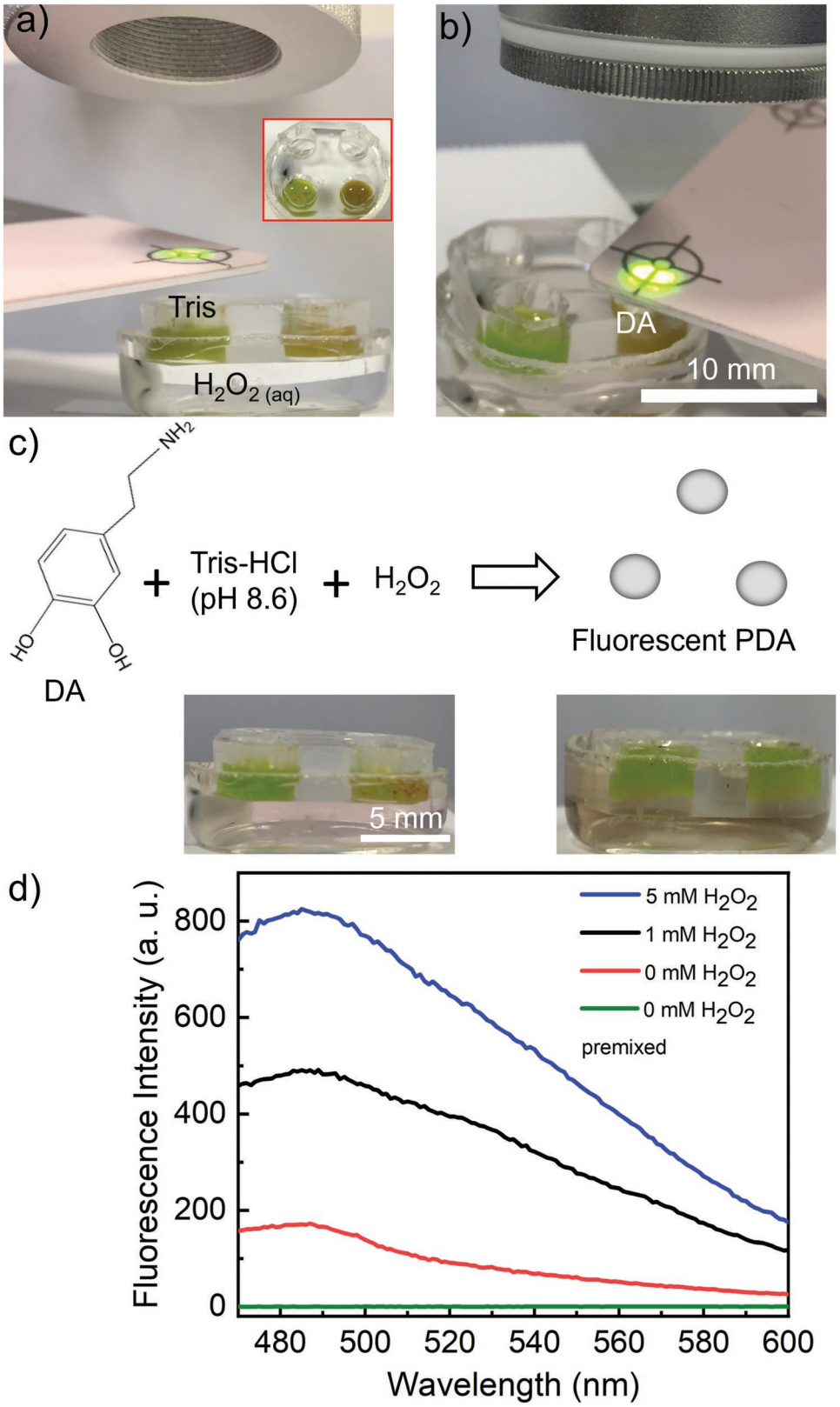

Figure 5. a) Water-in-LC emulsion loaded with Tris-HCl buffer droplets on the left mini-well excited with NIR laser. Green spot indicates the NIR laser beam. Inset: Top-view of the mini-wells filled with the emulsions loaded with Tris-HCl buffer and DA droplets. b) Water-in-LC emulsion loaded with DA droplets on the right mini-well excited with NIR laser. c) Oxidation reaction of DA in Tris-HCl buffer in the presence of H_2O_2. Pictures show the aqueous solutions during the release of DA and Tris buffer and after PDA formation. d) Fluorescence spectra of the in situ formed PDA in the absence and presence of H_2O_2 with concentration of 1×10^{-3} and 5×10^{-3} M and the fluorescence of PDA measured after premixing and incubation of DA and Tris-HCl buffer.

of DA with buffer quenches the fluorescence causing loss of sensitivity against H_2O_2 (Figure 5d). Therefore, it was critical to store DA and buffer in isolated wells and mix on-demand, which we showed herein as a successful application using the water-in-LC emulsion release system. Notably, laser-based heating adds value to the serially managed processes and holds significant advantage over chemical stimuli that trigger the release by diffusing to the sites unselectively.

Microcapsules, particles, and droplets have been the workhorses of photothermal therapy, drug release, and bioimaging since their size and shape fulfill the circulation, delivery, and uptake criteria in biological paths. Thus, in the last part of this study, we investigated the potential of the water-in-LC-in-water double emulsions in on-demand release. We prepared a double emulsion by dispersing the water(dyed)-in-LC emulsion in aqueous phase as large hybrid droplets (**Figure 6**a). The diameters of the hybrid droplets were kept around 1–3 mm to monitor the release characteristics visually under local heating. Droplets were positioned at the bottom of the aqueous solution and observed to yield a hemispherical shape (Figure 6a). Red water microdroplets in the hybrid LC droplets were mostly packed on the top regions due to the buoyancy effect. When the LC droplet was illuminated with a 1 mm-spot sized beam on its side (heated from the right edge in Figure 6b), water droplets within the LC were ejected from the top after gradually increasing the beam intensity from ≈23 to 70 W cm^{-2} (Figure 6e,f; Figure S9, Supporting Information). Surprisingly, ejection of the water droplets continued during the entire illumination duration revealing a continuous release mode that is distinct from the pulsated-mode described above for the release medium casted in mini-wells.

While the laser was illuminated on the right side of the droplet as shown in Figure 6b, water droplets in the LC medium were observed to flow counterclockwise (Video S2, Supporting Information). The internal flow was ascribed to the convectional heat transfer generated by the temperature gradient within the LC medium (Figure 6f). The magnitude of the temperature gradient was important in continuous-mode release since we observed a slowing down of the flow that led to the release termination when the illumination intensity was reduced to ≈40 W cm^{-2} as shown in Figure 6c,d. We observed the initiation of release after increasing the intensity back to 70 W cm^{-2} (Video S2, Supporting Information). As a control experiment, we illuminated the LC droplet with a 3 mm-spot sized beam and observed an absence of release at ≈8 W cm^{-2}, corresponding to the power (525 mW) close to that (550 mW) where we started to observe release with 1 mm-spot sized beam (Figure S9, Supporting Information). Because the internal flow was observed to be weaker due to the lower laser intensity compared to that generated by a 1 mm-spot sized beam (Video S3, Supporting Information). These observations revealed that a stronger internal flow formed in the LC droplet, induces a shear to the LC-aqueous phase boundary leading to microdroplet release by breaking the elastic energy barrier. Here we note that the shear-induced release, although with a different mechanism, was also observed in a past work showing the droplet release due to the external shear applied by the bacterial motion at the LC-aqueous phase interfaces.[26] Attractive electrical double layer interactions were used in that study to facilitate the release in addition to shear induced by bacterial motion.[26] However, we measured a zeta potential of −39.6 ± 3.0 mV for LC-aqueous interface and −85.6 ± 13.6 mV for LC-aqueous droplet interface of our system revealing a

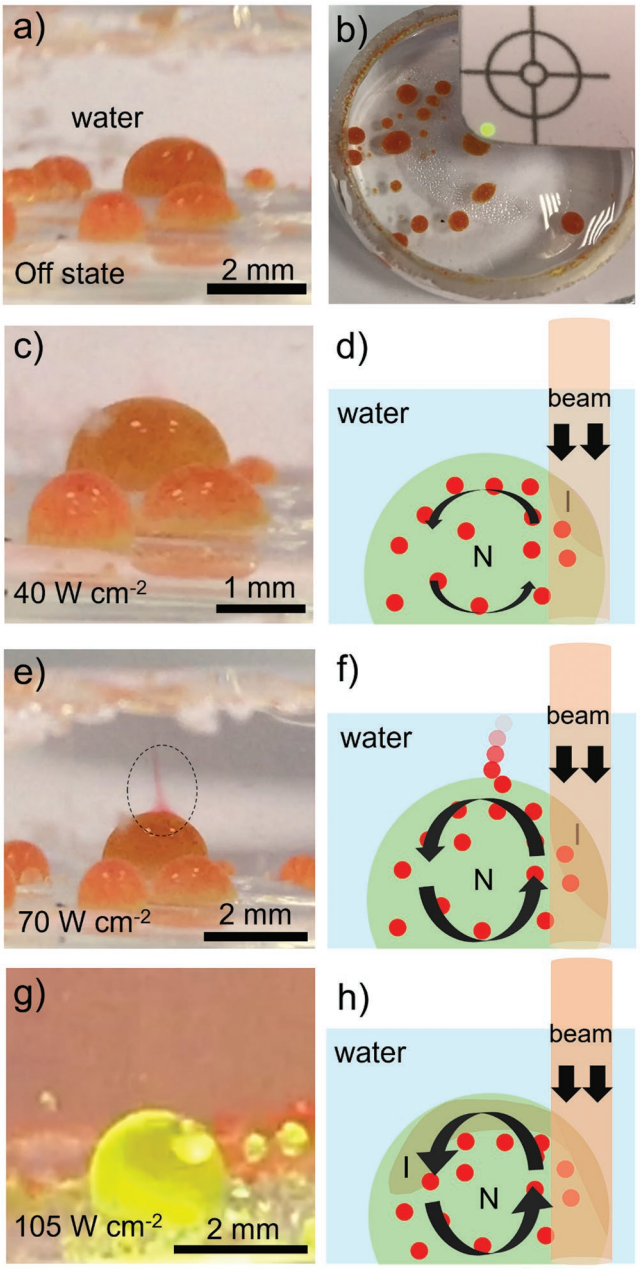

Figure 6. a) Large-sized droplet-shaped water (dyed)-in-LC immersed in aqueous solution at laser-off state. b) Illumination of LC droplet locally at its right edge with a 1 mm-spot sized beam. Green spot indicates the NIR laser beam. c) Photograph of an LC droplet upon exposure to laser beam at an intensity of 40 W cm^{-2} showing no release. d) Schematic representation of the low-speed internal flow because of the relatively low laser intensity. e) Photograph of an LC droplet upon exposure to laser beam at an intensity of 70 W cm^{-2} showing the continuous-mode release of the dyed aqueous droplets. f) Schematic representation of microdroplet release induced by internal flow. g) Photograph of an LC droplet upon exposure to laser beam at an intensity of 100 W cm^{-2} showing the cessation of the release due to bulk flow of I and N phases. h) Schematic representation of the internal structure of the LC droplet during the bulk flow. I and N represent the isotropic and nematic phases, respectively.

significant repulsive electrostatic interactions. We reasoned that this repulsive force plays a significant role in determining the onset of the continuous release-mode of the droplets, which we here report to happen above a certain NIR light intensity. Thus, our system demonstrates the significance of the laser-induced shear that is sufficient to promote the release despite the presence of the repulsive electrostatic forces. Although there are significant differences, the complete mechanism of this continuous release is not yet fully understood and requires further investigation. In the scope of our next study, we are currently studying light-induced flow strength and patterns and the role of electrostatic interactions, in motivation to provide a detailed insight of how the flow-induced microscopic and interfacial events lead to such a unique continuous release.

Importantly, light intensities above 100 W cm^{-2} using a 1 mm-spot sized beam in motivation to enhance the release rates with stronger flow resulted in the induction of a bulk flow of the isotropic and nematic phases as shown in Figure 6g,h (additional visuals are available in Video S2 and Figure S9, Supporting Information). Such flow appeared to hinder the transport of the LC-dispersed water microdroplets toward the LC-aqueous phase interface and resulted in termination of the release despite the strong flow. Such observations revealed the importance of an intermediate laser intensity range that permits both the droplet migration towards the LC-aqueous phase interface and generation of the shear force to break the elastic LC strains. It is noteworthy to highlight that such a convection-based release from droplet-shaped LC can only be achieved with localized stimulation by remote sources (e.g., light). Such continuous release presents a unique mechanism in the sense of instantaneous adjustment of excitation and excellent in situ on/off control in a single exposure with no wait time as in the diffusion-mediated or phase change processes. Thus, continuous-mode renders the LC-based release system versatile with a high spatiotemporal sensitivity developed using a single type of stimulation source.

3. Conclusion

We developed a stimuli-responsive droplet release mechanism using thermotropic LCs. A lyophilic photothermal dye that was physically hybridized with LC produced heat by NIR laser excitation, and the heating rate was tuned by adjusting the laser intensity and dye concentration. Photothermally-generated heat was exploited to deform elastic strains in LC and allow the initially entrapped aqueous microdroplets to merge with the bulk aqueous phase. Droplet release was modulated in two distinct ways (pulsated- and continuous) with high spatiotemporal resolution by LC geometry design, heating localization, and heating rate control. Released dosage was precisely regulated by tuning the LC dimensions, laser beam spot size, and laser on/off cycles. Dye-LC hybrid showed robust thermal stability under repeated heating cycles and multiple-time use. For continuous-mode release, we found an intermediate laser intensity regime critical to transport the microdroplets to the LC-aqueous interface and to generate shear for their release. Contactless, NIR-mediated stimulation we report here enabled a significantly rapid adjustment of the release by laser intensity and has the potential to lead to a breakthrough in the advancement of the LC-based materials for critical applications in drug release, controlled mixing, micro-scale-controlled synthesis and photothermal therapy among the others.

4. Experimental Section

Synthesis of PDIB Dye: PDIB was produced via the oxidation and ion exchange reactions of neutral amine (IPA) according to the previously reported method.[46] *N*,*N*,*N*″,*N*″-tetrakis(*p*-diisobutylaminophenyl)-*p*-phenylenediamine (1 g) was first added to a three-neck glass flask. Then, lithium bis(oxalate)borate (500 mg), dichloromethane (3.5 mL), and ethanol (2.5 mL) were added, and the mixture was refluxed for 2 h. Afterwards, sodium persulfate (330 mg) and deionized (DI) water (6.7 mL) were added, and the mixture was refluxed for further 2 h. The reaction was terminated by adding dichloromethane (150 mL) and DI water (200 mL). The mixture was vigorously shaken to transfer the unreacted species to water. The organic phase in the mixture was separated from the aqueous phase by using a separatory funnel. Dichloromethane in the organic phase was completely evaporated by using a rotary evaporator. PDIB dye was obtained as a dark green powder.

Preparation of Photothermal PDIB-5CB Hybrids: PDIB (20 mg) was dissolved in toluene (1 mL). Different portions of PDIB solution were mixed with 5CB (100 µL) to have LCs with final PDIB concentration of 0.075, 0.15, 0.3, 0.6, and 1.2 wt.%. The mixtures were ultrasonicated for 10 min to dissolve 5CB completely in toluene and then toluene was evaporated in vacuum oven overnight.

Photothermal Measurements: Fiber-coupled diode laser (CNI lasers, MDL-III-915-1 W) was used for all photothermal excitations at 915 nm and a thermal camera (FLIR Systems, Thermovision A40) was used to record the temperature of the PDIB-5CB hybrid mixtures. PDMS mini-wells were filled with PDIB-5CB (20 µL) and placed under laser aperture at a 10 cm distance. Laser beam spot size was adjusted to 3 mm. After the laser was turned on, temperature was recorded for 120 s. Laser power was adjusted to 62, 124, 186, and 248 mW for the measurement at different power intensities. For the measurements with different dye concentration, power and beam spot size were adjusted to 124 mW and 3 mm, respectively, and LCs with 0.075, 0.15, and 0.3 wt.% PDIB were measured. LC without PDIB was also measured as a control sample.

Preparation of PDMS Molds: Sylgard elastomer base (10 g) was mixed with curing agent (1 g) and degassed in a vacuum oven followed by casting on a glass petri dish. The mixture was cured at 100 °C for 10 min. Two 1 × 1 cm^2 PDMS pieces were cut, and circular holes of 5 mm and 3 mm diameter were punched at their centers using biopsy punches. A 6 × 6.5 mm square hole was created on a different 1 × 1 cm^2 PDMS piece using a razor blade.

Release Experiments: For release experiments, 5CB including 0.15 wt.% PDIB was used. First, red ponceau dye (20 mg) was dissolved in SDS solution (0.5 mL, 9×10^{-3} M). Note that 2.5 µL of that was added to PDIB-5CB (47.5 µL) and vortexed at 3000 rpm for 1 min to obtain water-in-PDIB/5CB emulsion with 5 vol.% water droplet. Prepared PDMS mini-wells were placed on the opening of spectrophotometry cuvettes (4 mL-volume) filled with water. Water-in-PDIB/5CB emulsions were drop-casted on water through the holes in a final thickness of 1 mm. Cuvettes were placed under laser aperture at a 10 cm distance. Beam spot size was adjusted to 9 mm and laser power was set as 460 mW. Release of the red dye to water was monitored visually after the laser was turned on. After the release was completed, laser was turned off. A calibration curve of absorbance at 506 nm versus red ponceau dye concentration (mg mL^{-1} water) was previously generated. After the release, absorbance of red dye was measured at 506 nm. Released dye mass (µg) in the 4 mL solutions was determined using the formula:

$$\text{Released mass}(\mu g) = \text{Concentration found in the calibration curve}\left(\text{mg mL}^{-1}\right) \times 4(\text{mL}) \times 1000\ \mu g\ \text{mg}^{-1} \quad (1)$$

Laser on/off cycles were repeated seven times and absorbance was measured after every release pulse. For the release measurements for different LC thicknesses, mini-wells of 3 mm diameter were filled with 10, 20, and 30 µL of the emulsions to have thicknesses of 1, 2, and 3 mm, respectively. A PDMS mold with 1.2 × 1.2 cm square hole was placed on the opening of a 5 mL beaker filled with water and 200 µL of the emulsion was drop-casted on water through the hole. The LC emulsion was first excited with 3 mm-spot sized beam with a power of 69 mW to have an intensity of 0.9 W cm^{-2} and the released mass was measured after seven on/off cycles. Experiments were repeated with 5 and 7 mm-spot sized laser beam with a power of 143 and 287 mW, respectively to obtain power intensity of 0.7 W cm^{-2}.

Preparation of Droplet-Shaped LC: Water-in-PDIB/5CB emulsion was vortexed in water at 1000 rpm for 5 s to form water-in-LC-in-water double emulsion and poured into a glass reservoir filled with water.

Hydrogen Peroxide (H_2O_2) Assay: Mini-wells were prepared by punching holes of 5 mm diameter and 4 mm height on a PDMS piece. PDMS was placed on the top of a glass dish filled with H_2O_2 solution (1×10^{-3} M). SDS (9×10^{-3} M) was prepared in Tris-HCl buffer (0.5 mL, 500×10^{-3} M, pH 8.6) and red ponceau (5 mg) was added. Ten microliters of that solution was vortexed in PDIB-5CB (90 µL) to have a droplet concentration of 10 vol.% and finally the emulsion was drop-casted in one mini-well. SDS (9×10^{-3} M) was prepared in DA solution (0.5 mL, 100×10^{-3} M) and red ponceau (5 mg) was added. Ten microliters of that solution was vortexed in PDIB-5CB (90 µL) and the emulsion was drop-casted in a second mini-well. First, the Tris-HCl mini-well was excited with a 6 mm-spot sized laser beam with a power of 69 mW. Then, the power was gradually increased to 282 mW to ensure that the LC phase turned to isotropic at the LC-aqueous interface. Droplet release was monitored with the help of the red tracer dye. Droplets were completely released after five successive heating and cooling steps. After buffer release, DA droplets were released similarly. After 3 h incubation at room temperature, fluorescence of the produced polydopamine was measured. Experiments were repeated in the absence and presence of H_2O_2 with a concentration of 5×10^{-3} M.

Characterization: Fluorescence measurements were done using a fluorescence spectrophotometer (Varian Eclipse). Polydopamine solutions were excited at 420 nm. Absorption signals of the PDIB dye, released red ponceau dye, and PDIB-5CB films were recorded using an UV–vis–NIR absorption spectrophotometer (Varian Eclipse, Cary 5000). PDIB-5CB films were prepared as a sandwiched structure between two glass slides by capillary suction. Thermographs of the PDIB-5CB hybrid mixtures were recorded using a differential scanning calorimeter (Perkin Elmer, DSC8000) with a scan rate of 5 °C min^{-1} at nitrogen atmosphere. Decomposition temperature of PDIB was measured using a thermogravimetric analyzer (TA Instruments, Q500) with a scan rate of 10 °C min^{-1} at nitrogen atmosphere. Zeta potential measurements were done by using Zetasizer Ultra (Malvern Instruments Ltd., US). Three independent measurements were collected from bare 5CB (1 µL mL^{-1}) droplets in water and in red ponceau dye-doped, 9×10^{-3} M SDS solutions and reported as averages and standard deviations. Droplets were sonicated for 10 min and equilibrated prior to measurements. Optical microscopy characterization was performed by using an Olympus BX53 microscope (Japan) equipped with 4×, 10×, and 50× objectives and crossed polarizers. The bright field (BF) and polarized (PL) micrographs were collected in transmission mode.

Statistical Analysis: The sample sizes and error bars are defined in the figure captions. The data were reported as average ± standard deviation.

Supporting Information

Supporting Information is available from the Wiley Online Library or from the author.

Acknowledgements

This work was supported by the Scientific and Technological Research Council of Turkey (TÜBİTAK) BİDEB-National Postdoctoral Research Program under the Project No. 118C462. The authors thank Dr. Selda Sezer for their help in zeta potential measurements.

Conflict of Interest

The authors declare no conflict of interest.

Data Availability Statement

The data that support the findings of this study are available from the corresponding author upon reasonable request.

Keywords

droplet release, drug delivery, liquid crystals, NIR light, photothermal heating

Received: May 11, 2022
Revised: July 22, 2022
Published online: August 24, 2022

[1] J. Liu, C. Detrembleur, S. Mornet, C. Jerome, E. Duguet, *J. Mater. Chem. B* **2015**, *3*, 6117.
[2] Z. Li, E. Ye, R. L. David, X. J. Loh, *Small* **2016**, *35*, 4782.
[3] S. Senapati, A. K. Mahanta, S. Kumar, P. Maiti, *Signal Transduction Targeted Ther* **2018**, *3*, 7.
[4] A. Raza, U. Hayat, T. Rasheed, M. Bilal, H. M. Iqbal, *J. Mater. Res. Technol.* **2019**, *8*, 1497.
[5] X. Fu, L. Hosta-Rigau, R. Chandrawati, J. Cui, *Chem* **2018**, *4*, 2084.
[6] X. Li, C. Xie, H. Xia, Z. Wang, *Langmuir* **2018**, *34*, 9974.
[7] M. Qiu, D. Wang, W. Liang, L. Liu, Y. Zhang, X. Chen, D. K. Sang, C. Xing, Z. Li, B. Dong, F. Xing, D. Fan, S. Bao, H. Zhang, Y. Cao, *Proc. Natl. Acad. Sci. USA* **2018**, *115*, 501.
[8] S. Geng, H. Zhao, G. Zhan, Y. Zhao, X. Yang, *ACS Appl. Mater. Interfaces* **2020**, *12*, 7995.
[9] M.-C. Chen, H.-A. Chan, M.-H. Ling, L.-C. Su, *J. Mater. Chem. B* **2017**, *5*, 496.
[10] M.-C. Chen, Z.-W. Lin, M.-H. Ling, *ACS Nano* **2016**, *10*, 93.
[11] Y. Dai, J. Su, K. Wu, W. Ma, B. Wang, M. Li, P. Sun, Q. Shen, Q. Wang, Q. Fan, *ACS Appl. Mater. Interfaces* **2019**, *11*, 10540.
[12] Q. Wang, Y. Dai, J. Xu, J. Cai, X. Niu, L. Zhang, R. F. Chen, Q. M. Shen, W. Huang, Q. Fan, *Adv. Funct. Mater.* **2019**, *29*, 1901480.
[13] Y. Zhang, G. Jiang, W. Hong, M. Gao, B. Xu, J. Zhu, G. Song, T. Liu, *ACS Appl. Bio Mater.* **2018**, *1*, 1906.
[14] J. Liu, C. Detrembleur, M.-C. De Pauw-Gillet, S. Mornet, L. V. Elst, S. Laurent, C. Jérôme, E. Duguet, *J. Mater. Chem. B* **2014**, *2*, 59.
[15] J. Ping, L. Qi, Q. Wang, S. Liu, Y. Jiang, L. Yu, J.-M. Lin, Q. Hu, *Biosens. Bioelectron.* **2021**, *187*, 113313.
[16] M. Tsuei, H. Sun, Y.-K. Kim, X. Wang, N. C. Gianneschi, N. L. Abbott, *Langmuir* **2022**, *38*, 332.
[17] W. Wu, W. Wang, L. Qi, Q. Wang, L. Yu, J. M. Lin, Q. Hu, *Anal. Chem.* **2021**, *93*, 6151.
[18] P. Bao, D. A. Paterson, P. L. Harrison, K. Miller, S. Peyman, J. C. Jones, J. Sandoe, S. D. Evans, R. J. Bushby, H. F. Gleeson, *Lab Chip* **2019**, *19*, 1082.

[19] X. Wang, H. Sun, Y.-K. Kim, D. B. Wright, M. Tsuei, N. C. Gianneschi, N. L. Abbott, *Adv. Mater.* **2022**, *34*, 2106535.
[20] O. M. Wani, R. Verpaalen, H. Zeng, A. Priimagi, A. P. H. J. Schenning, *Adv. Mater.* **2019**, *31*, 1805985.
[21] Y. Wu, Y. Yang, Q. Chen, X. Qian, Y. Wei, Y. Ji, *Angew. Chem., Int. Ed.* **2020**, *59*, 4778.
[22] L. L. Dong, Y. Zhao, *Mater. Chem. Front.* **2018**, *2*, 1932.
[23] U. Manna, D. M. Lynn, *Adv. Mater.* **2015**, *27*, 3007.
[24] F. Lancia, A. Ryabchun, N. Katsonis, *Nat. Rev. Chem.* **2019**, *3*, 536.
[25] C. Esteves, E. Ramou, A. R. P. Porteira, A. J. Moura Barbosa, A. C. A. Roque, *Adv. Opt. Mater.* **2020**, *8*, 1902117.
[26] Y.-K. Kim, X. Wang, P. Mondkar, E. Bukusoglu, N. L. Abbott, *Nature* **2018**, *557*, 539.
[27] D. Franklin, T. Ueltschi, A. Carlini, S. Yao, J. Reeder, B. Richards, R. P. Van Duyne, J. A. Rogers, *ACS Nano* **2021**,*15*, 2327.
[28] D. Zhao, F. Fan, J. Cheng, Y. Zhang, K. S. Wong, V. G. Chigrinov, H. S. Kwok, L. Guo, B. Z. Tang, *Adv. Opt. Mater.* **2015**, *3*, 199.
[29] A. Hou, H. Chen, C. Zheng, K. Xie, A. Gao, *ACS Nano* **2020**, *6*, 7380.
[30] Y. Xu, A. M. Rather, Y. Yao, J. C. Fang, R. S. Mamtani, R. K. A. Bennett, R. G. Atta, S. Adera, U. Tkalec, X. Wang, *Sci. Adv.* **2021**, *7*, eabi7607.
[31] A. H. Gelebart, D. Q. Liu, D. J. Mulder, K. H. J. Leunissen, J. van Gerven, A. P. H. J. Schenning, D. J. Broer, *Adv. Funct. Mater.* **2018**, *28*, 1705942.
[32] Y. Zhan, G. Zhou, B. A. G. Lamers, F. L. L. Visschers, M. M. R. M. Hendrix, D. J. Broer, D. Liu, *Matter* **2020**, *3*, 782.
[33] L. Pezzi, L. De Sio, A. Veltri, T. Placido, G. Palermo, R. Comparelli, M. L. Curri, A. Agostiano, N. Tabiryan, C. Umeton, *Phys. Chem. Chem. Phys.* **2015**,*17*, 20281.
[34] L. De Sio, P. F. Lloyd, N. V. Tabiryan, T. Placido, R. Comparelli, M. L. Curri, T. J. Bunning, *ACS Appl. Nano Mater.* **2019**, *2*, 3315.
[35] N. Podoliak, O. Buchnev, O. Buluy, G. D'Alessandro, M. Kaczmarek, Y. Reznikov, T. Sluckin, *Soft Matter* **2011**, *7*, 4742.
[36] Y. Ji, F. Fan, S. Xu, J. Yu, S. Chang, *Nanoscale* **2019**, *11*, 4933.
[37] Y. Tao, H. F. Chan, B. Y. Shi, M. Q. Li, K. W. Leong, *Adv. Funct. Mater.* **2020**, *30*, 2005029.
[38] H. T. Sun, M. X. Feng, S. Y. Chen, R. Z. Wang, Y. Luo, B. Yin, J. C. Li, X. L. Wang, *J. Mater. Chem. B* **2020**, *8*, 7149.
[39] W. J. Jiang, F. Mo, X. Jin, L. Chen, L. J. Xu, L. Q. Guo, F. F. Fu, *Adv. Mater. Interfaces* **2017**, *4*, 1700425.
[40] A. Wang, Q. Mao, M. Zhao, S. Ye, J. Fang, C. Cui, Y. Zhao, Y. Zhang, Y. Zhang, F. Zhou, H. Shi, *Anal. Chem.* **2020**, *92*, 16113.
[41] H. Zeng, P. Wasylczyk, D. S. Wiersma, A. Priimagi, *Adv. Mater.* **2017**, *30*, 1703554.
[42] J. Li, R. Zhang, L. Mou, M. Jung de Andrade, X. Hu, K. Yu, J. Sun, T. Jia, Y. Dou, H. Chen, S. Fang, D. Qian, Z. Liu, *Adv. Funct. Mater.* **2019**, *29*, 1808995.
[43] B. Zuo, M. Wang, B. P. Lin, H. Yang, *Nat. Commun.* **2019**, *10*, 4539.
[44] S. B. Chernyshuk, B. I. Lev, *Phys. Rev. E* **2011**, *84*, 011707.
[45] P. Poulin, H. Stark, T. C. Lubensky, D. A. Weitz, *Science* **1997**, *275*, 1770.
[46] M. Han, B. Kim, H. Lim, H. Jang, E. Kim, *Adv. Mater.* **2020**, *32*, 1905096.
[47] A. Y. Rwei, W. Wang, D. S. Kohane, *Nano Today* **2015**, *10*, 451.
[48] J. Vapaavuori, A. Siiskonen, V. Dichiarante, A. Forni, M. Saccone, T. Pilati, C. Pellerin, A. Shishido, P. Metrangolo, A. Priimagi, *RSC Adv.* **2017**, *7*, 40237.
[49] J. W. Liu, Y. Luo, Y. M. Wang, L. Y. Duan, J. H. Jiang, R. Q. Yu, *ACS Appl. Mater. Interfaces* **2016**, *8*, 33439.
[50] Z. Song, R. T. Kwok, D. Ding, H. Nie, J. W. Lam, B. Liu, B. Z. Tang, *Chem. Commun.* **2016**, *52*, 10076.
[51] J. Chang, H. Li, T. Hou, W. Duan, F. Li, *Biosens. Bioelectron.* **2018**, *104*, 152.
[52] T. G. Barclay, H. M. Hegab, S. R. Clarke, M. Ginic-Markovic, *Adv. Mater. Interfaces* **2017**, *4*, 1601192.
[53] S. Hong, Y. S. Na, S. Choi, I. T. Song, W. Y. Kim, H. Lee, *Adv. Funct. Mater.* **2012**, *22*, 4711.
[54] J.-H. Lin, C.-J. Yu, Y.-C. Yang, W.-L. Tseng, *Phys. Chem. Chem. Phys.* **2015**, *17*, 15124.